
Article:
Yan, Jiexiong, Dawson, John F. orcid.org/0000-0003-4537-9977, Marvin, Andy C. orcid.org/0000-0003-2590-5335 et al. (2 more authors) (2019) 3D Diffusion Models for Predicting Reverberant Electromagnetic Fields in Loaded Enclosures. IEEE Transactions on Electromagnetic Compatibility. pp. 1362-1369. ISSN 0018-9375

https://doi.org/10.1109/TEMC.2019.2916820

3D Diffusion Models for Predicting Reverberant Electromagnetic Power Density in Loaded Enclosures

Jiexiong Yan, John F. Dawson, *Member*, *IEEE*, Andy C. Marvin, *Life Fellow*, *IEEE*, Ian D. Flintoft, *Senior Member*, *IEEE*, and Martin P. Robinson

***Abstract*-- The power balance technique for the prediction of shielding effectiveness of reverberant enclosures is fast and simple to use. However, it assumes a uniform field in the enclosure, which has been shown to be incorrect in the presence of dissipative contents. The diffusion model is a generalization of the power balance method that can account for the field inhomogeneity due to the presence of losses with much lower computational effort than a full wave solver. Evaluation of a 2D diffusion model produced promising results compared to physical measurements. Here we present a 3D diffusion model applied to an enclosure with an aperture and dissipative contents. Comparisons between the 3D diffusion model, measurements and a full wave solver suggest that it is able to account for the variation of the electromagnetic field due to dissipative contents with far less computational effort than full wave solvers. The diffusion model allows rapid solution of the shielding effectiveness of enclosures with dissipative contents and arbitrary geometries. and reduces the time to model equipment enclosures from hours to minutes, whilst still determining the variation of field strength due to contents. In addition, the method may help predict field inhomogeneity in reverberation chambers.**

***Index Terms*-- Diffusion model, enclosure shielding, power balance, reverberation chamber, shielding effectiveness**

I. Introduction

PREDICTION of the electromagnetic fields in electrically large enclosures is a difficult problem. Full wave simulations, which are based on Maxwell's equations, are one possible solution [1-4]. However, they can be extremely costly in terms of computational resources when applied to electrically large enclosures [5].

A widely used technique to analyze the electromagnetic field inside electrically large enclosures with contents is the power balance (PWB) method [6] [7]. This method evaluates the electromagnetic fields from the electromagnetic power density. It assumes that the enclosure under test is electrically large with a uniform power density. In the steady state, the power that enters the enclosure is equal to the power dissipated inside. If the enclosure contains an aperture, an antenna and some contents, then the dissipated power can be divided into wall loss, aperture leakage, contents and antenna absorption. In this way, a large, complex system is replaced by several smaller ones and the problem is simplified. When using PWB, an aperture is characterized by its transmission cross section (TCS); walls and contents are represented by their absorption cross sections (ACS). The shielding effectiveness of the enclosure, defined as the ratio of the external and internal power densities, can be easily calculated from the ACS and TCS [8]. The advantage of the PWB method is that it does not require knowledge of the detailed geometry of the contents or enclosure since it only considers average energy density in the enclosure. When the losses are low, multiple reflections from the walls and contents make the power density in the enclosure uniform when averaged over the full range of possible illuminations. When the losses are moderate or high, the internal power density is no longer uniform and the PWB method does not consider this inhomogeneity.

The acoustic community has developed a diffusion based model that is able to account for the variation of a reverberant acoustic field in an enclosure due to the presence of high losses. The latest development of the diffusion model can be found in [9] and [10]. The diffusion method stems from the radiative transport theory of rays in an enclosure and can be seen as a generalization of the PWB method. Although the computational cost of the diffusion model is higher than that of the PWB method, it is still much lower than that of full wave solvers. Flintoft et al. have translated the acoustic formalism to an electromagnetic formalism and discussed its relationship to the PWB and full-wave methods [11]. For the initial evaluation, they constructed 2D diffusion models of single and dual coupled enclosures. In both models, an absorbing cylinder served as content. The simulations generally agree with experimental results. However, the 2D model is only suitable to structures with constant cross sections so its applicability is limited.

In this paper, which is an extended version of our conference paper [12], we present a 3D diffusion model of an enclosure and compare the results to full wave simulations and measurements. The main differences between our study and that in [11] are: first, the enclosure we use contains an aperture, which makes it more realistic; and secondly the measurements were performed

Submitted for review 11th December 2018.
For Special Issue SINGAPORE & LONG BEACH 2018.

J. Yan, J. F. Dawson, A. C. Marvin, M. P. Robinson and are with the Department of Electronic Engineering, University of York, Heslington, York YO10 5DD, UK. (E-mails: jy936, john.dawson, andy.marvin, martin.robinson@york.ac.uk).

I. D. Flintoft is with SNC-Lavalin's Atkins Business, York YO1 6HZ, UK. (E-mail: ian.flintoft@googlemail.com).

in a reverberation chamber so that the external environment around the enclosure is reverberant. In Section II, we review the theory of the diffusion model in 3D. In Section III, we describe the details of the enclosure. Section IV explains the 3D diffusion model of the enclosure. Section V presents the full wave model of the enclosure. Section VI describes the measurement methodology. The results are presented in Section VII and we conclude in Section VIII.

II. Theory

A. The diffusion model

Flintoft et al. give a detailed review of the diffusion model in [11]. Here we present only the main features. The diffusion model assumes that there is a diffuse electromagnetic field in the space under test. The average volumetric energy density of the diffuse field at position $\mathbf{r}$ is:

$$w(\mathbf{r}) = \langle \frac{1}{2}[\varepsilon_0 E^2(\mathbf{r}) + \mu_0 H^2(\mathbf{r})] \rangle \quad (1)$$

where ε_0 and μ_0 are the vacuum permittivity and permeability, $E(\mathbf{r})$ and $H(\mathbf{r})$ are the total (RMS) electric and magnetic fields. The symbol <·> denotes an average of a statistical ensemble of fields due to, for instance, different sources of illumination or mechanical or frequency stirring in a reverberation chamber. The scalar power density $S(\mathbf{r})$ and the energy density $w(\mathbf{r})$ are related by:

$$S(\mathbf{r}) = cw(\mathbf{r}) \quad (2)$$

where c is the velocity of light. The scalar power density may be considered as the average power per unit area incident from all directions. The diffuse electromagnetic energy density $w(\boldsymbol{r})$ in a space with the volume of V satisfies the following equation:

$$(D\nabla^2 + \Lambda)w(\mathbf{r}) = P(\mathbf{r}) \quad (3)$$

where D is the diffusivity, Λ is the volumetric loss rate due to absorption in the medium filling the enclosure and P is the power radiated by any source at position $\mathbf{r}$. The volumetric loss rate Λ from the absorption of contents is calculated by [13]:

$$\Lambda = \frac{c\alpha_c}{l_c} \quad (4)$$

where α_c is the absorption efficiency of the contents and l_c stands for the contribution of contents to the mean free path. In our examples, there are surface losses only so Λ is zero.

The diffusivity D is related to the overall mean free path (MFP), l, between scatterings of rays from the walls and contents of the enclosure:

$$D = \frac{cl}{3} \quad (5)$$

The contribution to the mean free path due to the walls and contents are given by (6) and (7) respectively [14] [15]:

$$l_w = \frac{4V}{A_w} \quad (6)$$

$$l_c = \frac{4V}{A_c} \quad (7)$$

where A_w and A_c are the surface areas of the walls and contents and V is the volume of the enclosure. The overall mean free path is given by:

$$l^{-1} = l_w^{-1} + l_c^{-1} \quad (8)$$

On the boundary surface of the enclosure walls and contents, the energy density is assumed to satisfy a Robin boundary condition:

$$[D\hat{\mathbf{n}} \cdot \nabla + c\sum_\alpha(\mathbf{r})]w(\mathbf{r}) = 0 \quad (9)$$

where $\hat{\mathbf{n}}$ is the outward unit normal vector and $\sum_\alpha(\mathbf{r})$ is the absorption factor of the walls. The simplest estimation of $\sum_\alpha(\mathbf{r})$ is obtained by Sabine's formula [16]:

$$\sum_\alpha(\mathbf{r}) = \frac{\alpha_w(\mathbf{r})}{4} \quad (10)$$

where $\alpha_w(\mathbf{r})$ is the absorption efficiency of the walls. Flintoft et al pointed out that (10) is accurate only when $\alpha_w(\mathbf{r}) \le 0.2$ [13]. More recently, a formula based on a radiative transport model has been proposed which appears to give good results over the full range of absorption efficiency [17]:

$$\sum_\alpha(\mathbf{r}) = \frac{c\alpha_w(\mathbf{r})}{2(2-\alpha_w(\mathbf{r}))} \quad 0 \le \alpha_w(\mathbf{r}) \le 1 \quad (11)$$

This formula assumes that the reflection process of the walls is completely diffusive, for example, the power reflectance is independent of the incident angles. For low absorption cases in which $\alpha_w(\mathbf{r}) < 0.4$, (11) predicts close results to that of (10). For high absorption, however, the estimation of (11) approaches twice as that of (10). The enclosure we use has a very low absorption efficiency. Therefore, for simplicity, in our diffusion model we use (10) to calculate the absorption factor.

Visentin et al argue in [18] that the point source term in (3) gives rise to a spurious "direct" term due to the fact that a diffuse field has not been established in the close vicinity of the point source. This direct term should be removed to give the true reverberant density:

$$w_r(\mathbf{r}) = w(\mathbf{r}) - \frac{P}{4\pi D|\mathbf{r}-\mathbf{r}_s|} \quad (12)$$

In our diffusion model, we disregarded the power density within 50mm (which is about half the mean free path of the cavity) of the point source when considering (12). The details of the enclosure under test and its diffusion model will be presented in Section III and IV respectively.

B. Coupled cavities

In the diffusion model of dual cavities, a single or dual domain model can be used [11]. In this paper, we use a dual domain model. The enclosure under test and the reverberation chamber are represented by separate domains and are coupled by an aperture represented by a translucent part of the shared boundary. If the coupling between the two domains is not too large we can assume each of them satisfies a diffusion equation given by the single domain relationship (3). On the shared boundary, we apply the energy exchange boundary condition (EEBC) which enforces the Robin boundary condition of (9) as described in [19]:

$$\hat{\mathbf{n}}_1 \cdot [D_1(\mathbf{r})\nabla w_1(\mathbf{r})] + h_{11}(\mathbf{r})w_1(\mathbf{r}) - h_{12}(\mathbf{r})w_2(\mathbf{r}) = 0 \quad (13)$$

$$\hat{\mathbf{n}}_2 \cdot [D_2(\mathbf{r})\nabla w_2(\mathbf{r})] + h_{22}(\mathbf{r})w_2(\mathbf{r}) - h_{21}(\mathbf{r})w_1(\mathbf{r}) = 0 \quad (14)$$

where $\hat{\mathbf{n}}_i$, D_i and w_i (i=1,2) are the outward normal vector, diffusivity and energy density of their respective domains. The exchange coefficients h_{11} and h_{22} determine the power lost on their respective sides of the boundary while h_{12} and h_{21} determine the power coupled across the boundary from the other domain.

If the coupling surface is a lossless and reciprocal aperture with average transmission efficiency α_a then:

$$h_{ii} = \frac{c\alpha_a}{4} \quad \text{for } i = 1, 2 \quad (15)$$

In the geometric optics regime, the energy lost through an

Fig. 1. Photograph of the enclosure under test, showing the 75mm×75mm aperture. The holes along the central line of the lid are the measurement points. A diagram is provided in Fig.2.

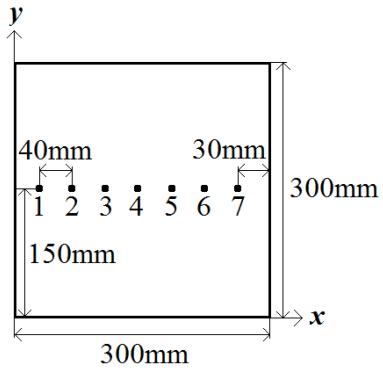

Fig. 2. Diagram of the measurement points in the lid of the enclosure shown in Fig.1.

aperture is indistinguishable from that absorbed in a perfect absorber of the same area.

C. Relationship between diffusion model and PWB method

If the energy density $w(\mathbf{r})$ in an enclosure is static and homogenous, and the wall absorption is also homogenous, then inserting Sabine's formula (10) and the loss rate formula (4) into the diffusion equation (3) reduces it to [11]:

$$\left(\frac{1}{4}\alpha_w A_w + \frac{1}{4}\alpha_c A_c\right) cw = P \tag{16}$$

The absorption efficiencies of the walls and contents are given by:

$$\alpha_w = \frac{4\sigma_w}{A_w} \tag{17}$$

$$\alpha_c = \frac{4\sigma_c}{A_c} \tag{18}$$

where σ_w and σ_c are the absorption cross sections (ACS) of the walls and contents respectively. Substituting (2), (17) and (18) into (16) we obtain the classic PWB relationship [6]:

$$(\sigma_w + \sigma_c)S = P \tag{19}$$

III. Test Geometry

Fig.2 shows the enclosure under test in this paper. It has dimensions of 300 mm × 300 mm × 120 mm. There is a 75 mm × 75 mm aperture at the center of the front face. The cut-off frequency of the aperture, which marks its transition from electrically small to electrically large, is 1GHz. We also measured the same enclosure with a circular aperture of radius 6mm (not shown in the photograph), which has a cut-off frequency of 10.2GHz. The lid of the enclosure is removable to allow access and it is fitted with gaskets to ensure good electrical contact. There are seven measurement positions in which a monopole probe can be installed. They are distributed along the central line of the lid at intervals of 40mm as shown in Fig. 2. The enclosure is made from the same material, brass sheet, as that in [6]. Therefore, we assume the enclosure walls to have the same absorption efficiency of α_w=0.0027.

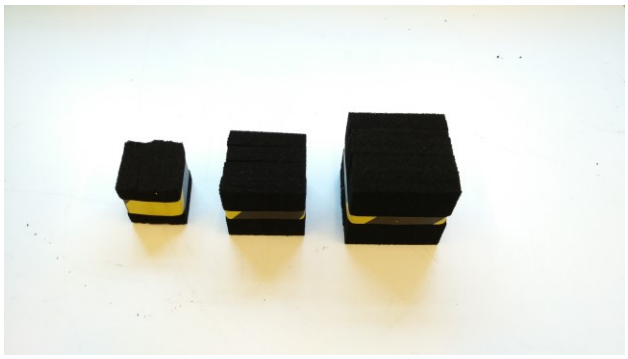

Fig. 3. Photograph of the absorbing cubes used for the measurements. Their side lengths are (from left to right) 55mm, 70mm and 90mm.

During the measurements a series of absorbing cubes were placed in the center of the enclosure. Fig.3 shows a photo of them. The absorbing cubes have side lengths of 55mm, 70mm and 90mm respectively. They are made from the same LS22 radio absorbing material as the cylinder in [11]. We have previously measured the ACS of the cubes in a reverberation chamber by using the method described in [20]. The absorption efficiency of the cubes was calculated using (18) and was found to be approximately α_c=0.95 above 2GHz. For the full wave solver the complex permittivity of the LS22 material was fitted to a three-pole Debye dispersion model [21]:

$$\hat{\varepsilon}_r = \varepsilon_\infty + \sum_{k=1}^{3} \frac{\Delta\varepsilon_k}{1+j\omega\tau_k} + \frac{\sigma_{DC}}{j\omega\varepsilon_0} \tag{20}$$

where ω is the angular frequency, $\varepsilon_\infty = 1.1725$, σ_{DC}=0.1mS/m, $\Delta\varepsilon_1$=1.04×10^{-3}, $\Delta\varepsilon_2$=17.9, $\Delta\varepsilon_3$=0.49, τ_1=55.3ms, τ_2=0.188ns, τ_3=6.2ps.

IV. 3D Diffusion Model

We use the FreeFEM++ software to build the 3D diffusion model [22]. The walls and contents of the enclosure are modeled by including their surfaces in the mesh and applying the Robin boundary condition (9), with the appropriate absorption efficiency.

Fig. 4 shows a diagram of the cross sectional view of the diffusion model. Enclosures A and B represent a reverberation chamber and the enclosure under test respectively. They are coupled through a shared boundary that is depicted by the dashed lines. The EEBC as described in (13) and (14) was used on it with a unity transmission efficiency. In the diffusion model the size of the reverberation chamber is not important as long as the aperture is an adequate distance from the point source as a diffuse field exists by definition. Here we use a small enclosure to represent the reverberation chamber to minimize the computational effort. An absorbing cube can be seen in the center of enclosure B and an isotropic point source is in enclosure A. The radiated power, P in (3), is 1W. Figs. 5 and 6

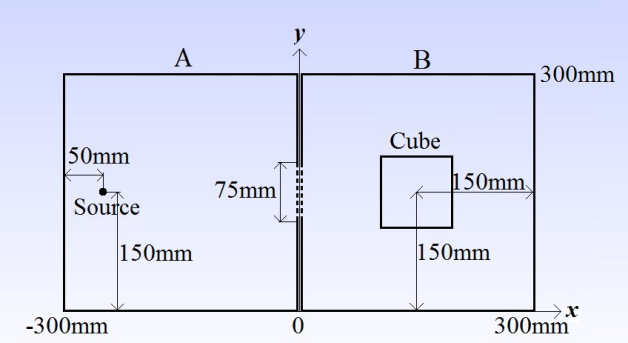

Fig. 4. Diagram of the cross sectional view at half height (z=60mm) of the 3D diffusion model. Enclosure A represents a reverberation chamber while B is the enclosure under test (shown in Fig.1). The dashed lines denote shared boundaries (the aperture) on which the EEBC are applied.

show the mesh of the diffusion model from different cross sections. Fig. 6 presents a cross sectional view at x=0 plane in order to show the shared boundary that represents the aperture.

In [11], Flintoft et al noted that in the diffusion model, the mesh size is determined by the mean free path rather than the wavelength and this property allows a much coarser mesh to be used in the diffusion model than in full wave simulation. The mesh size in our model is between 10mm and 30mm. All the FreeFEM++ results were obtained in less than 1 minute on a desktop computer (Intel Core i7-870 @2.93GHz, 8GB RAM), compared with up to 42 hours for the full wave model. The energy density and power density in the enclosure are calculated by (12) and (2) respectively.

The shielding effectiveness of the enclosure is defined as the ratio of the power density in the chamber (enclosure A) to that in the enclosure-under-test (enclosure B). Normally the chamber is sufficiently large and low loss that its power density is uniform, whereas the power density in the populated enclosure, and hence shielding effectiveness, varies with position as demonstrated below.

V. Full Wave Simulation

The full wave simulations were performed by using CST Microwave Studio (MWS) 2016 [23]. As mentioned in Section II, the use of the diffusion model requires a diffuse electromagnetic environment. In the measurements, this requirement was achieved by using a mechanical stirrer in a reverberation chamber. In the full wave solver, however, the presence of a stirrer would significantly increase the number of mesh cells and thus the simulation time. Therefore, we follow Flintoft et al and use a number of plane waves to illuminate the enclosure from different angles to create a reverberant field [21].

Flintoft et al used 64 plane waves, which was shown to give ±1 dB accuracy in average power quantities. In this paper, in order to save time, we use 36 plane waves. In Section VII, we will present an example to show that 36 and 64 plane wave produce very similar (within 1 dB difference) results for the current application.

Fig. 7 shows the CST MWS model of the enclosure. A line of probes was defined along the central line of the lid. Fig. 8 shows the top view of the lid, which gives a better view of the

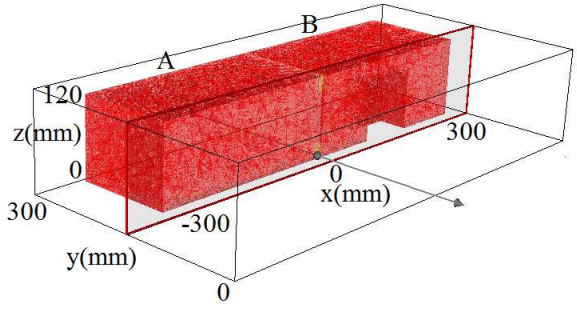

Fig. 5. Cross sectional view at half width (y=150mm) of the mesh of the 3D diffusion model. Enclosures A and B are in accordance with those in Fig.4. The hollow space in enclosure B represents the absorbing cube.

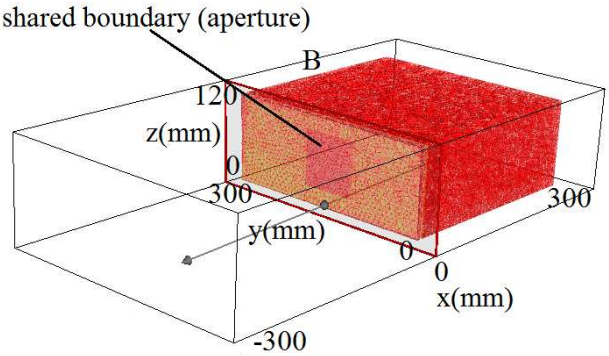

Fig. 6. Cross sectional view at x=0 of the mesh of the 3D diffusion model. Enclosure A is not included in order to show the shared boundary that represents the aperture.

probe positions. The probes record both electric and magnetic fields in x, y, and z directions and the power density can be calculated using (1) and (2). Comparing Fig. 2 and Fig. 8, it can be seen that the distance between the probes in CST MWS is half of that of the probes in the real enclosure. This is due to the fact that in CST MWS it takes no extra efforts to define a probe. Therefore, we put more probes in the CST model to get results with a higher resolution. By using the parametric sweep function, we let a number of plane waves illuminate the enclosure with their incident angles chosen by the method detailed in [21]. Considering the computation time and memory requirement, we only simulate the field from 1GHz to 10GHz. For the enclosure loaded with the 90mm, 70mm and 55mm absorbing cube, the full wave simulations took 10, 25 and 42 hours to finish respectively on the York Advanced Research Computing Cluster (YARCC) which has a variety of processor types (typically Intel E5-2760 v2 @ 2.5GHz with 16 cores) [24].

VI. Measurement Methodology

The validation measurements were performed in a reverberation chamber with dimensions of 4.7 m × 3 m × 2.37 m. Figs. 9 and 10 show a diagram and a photograph of the measurement configuration. We used the three-antenna method as recommended in the IEEE standard 299.1 [25]. A blade antenna (antenna 1) served as a radiation source [26]. A monopole (antenna 2) with a length of 10mm was fitted through each of the holes in the removable lid of the enclosure in turn, to measure the internal fields. An identical

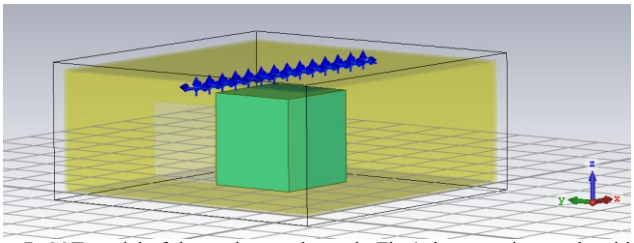

Fig. 7. CST model of the enclosure shown in Fig.1 that contains an absorbing cube, showing the 75mm×75mm aperture. A line of probes is along the central line of the lid.

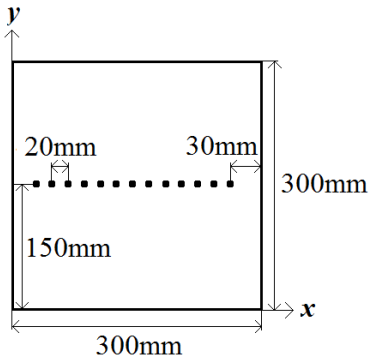

Fig. 8. Diagram of the positions of the probes in the CST model shown in Fig. 7.

monopole (antenna 3) was fitted at the center of a 480mm×480mm metal plane to measure the external field. The reverberation chamber was mode-tuned by a mechanical stirrer using 100 equally spaced positions over one complete rotation. First, we used a network analyzer to measure the S-parameters between antenna 1 and antenna 2, then between antenna 1 and antenna 3. The measurement range was 1GHz to 10GHz with 10001 equally spaced points. During the measurements, the unused holes on the enclosure lid were covered and the unused monopole (either antenna 2 or 3) was attached to a 50Ω load.

The mismatch corrected insertion gain between the radiation source and the receiving antennas was calculated from the S-parameters [11]:

$$IG_{1i} = \frac{\langle |S_{i1}|^2 \rangle}{(1-|\langle S_{11} \rangle|^2)(1-|\langle S_{ii} \rangle|^2)} \quad i = 2,3 \qquad (21)$$

where S_{21} and S_{31} are the transmission coefficients between the transmitting and receiving antennas. S_{11}, S_{22} and S_{33} are the refection coefficients of the three antennas respectively. The power densities in the reverberation chamber and the enclosure are proportional to the insertion gain so that:

$$\frac{IG_{13}}{IG_{12}} = \frac{S_{ch}}{S_{en}} \qquad (22)$$

where S_{ch} and S_{en} are the power densities in the chamber and in the enclosure respectively. This ratio is also the shielding effectiveness of the enclosure.

VII. Results

Fig.11 shows the variation of the calculated power density along the central line of the lid of the enclosure loaded with the 90 mm × 90 mm × 90 mm cube for different values of the cube's absorption efficiency α_c. The PWB method assumes a constant power density independent of position, whereas in the diffusion model the power density is greater near the aperture

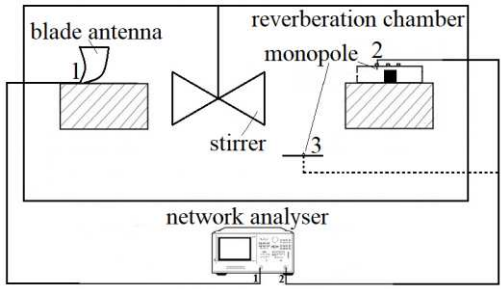

Fig. 9. Diagram of the configuration of the validation measurement. The measurements were performed in a reverberation chamber by using the three-antenna method. Antenna 1 is the radiation source, antenna 2 and 3 are monopoles fitted onto the enclosure and a metal plane respectively.

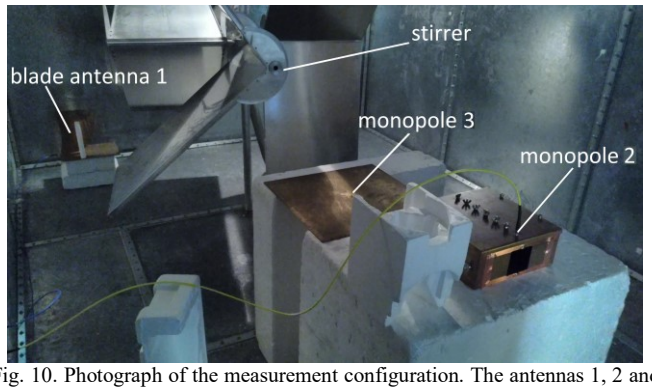

Fig. 10. Photograph of the measurement configuration. The antennas 1, 2 and 3 are in accordance with those shown in Fig.9.

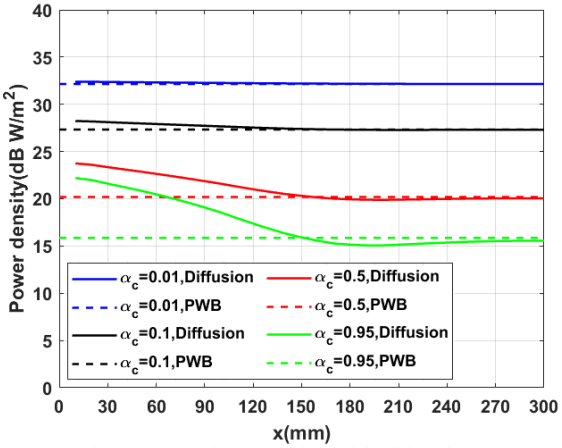

Fig. 11. Power density along the central line of the lid of the enclosure with the 90mm cube as a function of the cube's absorption efficiency α_c, comparing predictions between the diffusion model and the PWB method.

and reduces near the absorber. For α_c=0.01, the power density is relatively homogenous and the difference between the two predictions is less than 0.1 dB. As α_c increases, the discrepancy between them becomes more and more obvious, particularly at the front part of the enclosure (the space between the aperture and the cube, 0mm<x<120mm). At the rear part of the enclosure (the space behind the cube, 210mm<x<300mm), the diffusion model prediction gradually becomes close to that of the PWB method. This is, as we would expect, since the power balance, which must be true for both models, dictates that the energy density at the absorber surface must be the same in both models, as this determines the total energy absorbed.

Fig.12 shows the power density, predicted by CST MWS,

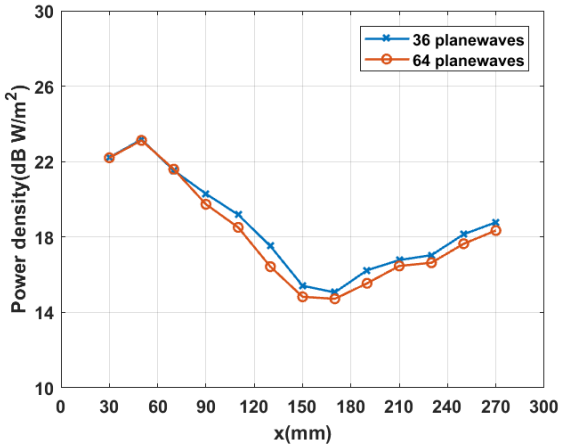

Fig. 12. CST predictions of the power density, normalized to 1W input power, along the central of the lid of the enclosure with the 90mm cube at 5.5 GHz obtained by using different numbers of plane waves.

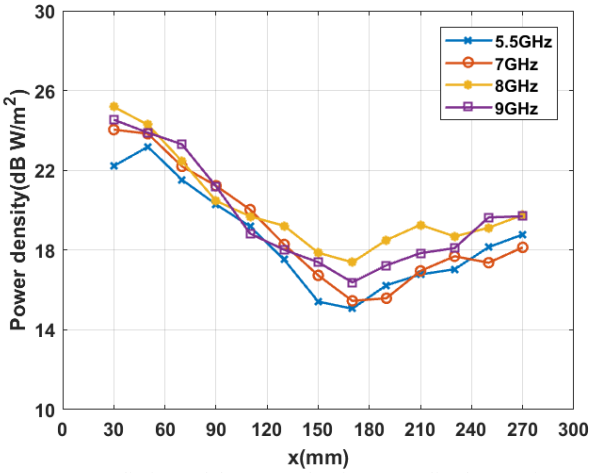

Fig. 13. CST predictions of the power density, normalized to 1W input power, along the central of the lid of the enclosure with the 90mm cube at different frequencies.

along the central line of the enclosure loaded with the 90 mm × 90 mm ×90 mm cube. The simulations were performed using 36 and 64 plane waves respectively as discussed in Section V. The two full wave simulations produced very similar results with a difference of less than 1 dB. Therefore, in order to save time, all the subsequent CST simulations were performed by using 36 plane waves.

Fig.13 shows the CST MWS prediction of the power density along the central line of the lid of the enclosure loaded with the 90 mm × 90 mm × 90 mm cube at a number of different frequencies. Comparing the power densities at 5.5GHz, 7GHz, 8GHz and 9GHz, we can see that they are generally in agreement with less than 3 dB difference. For simplicity, in the following results we only plot the power density at 5.5GHz.

Figs.14-16 show the power densities along the central line of the lid of the enclosure when loaded with the three different cubes. In order to compare with the diffusion model predictions, all the results obtained from full wave simulations and measurements were normalized to 1W input power. The diffusion model predictions are generally in agreement with full

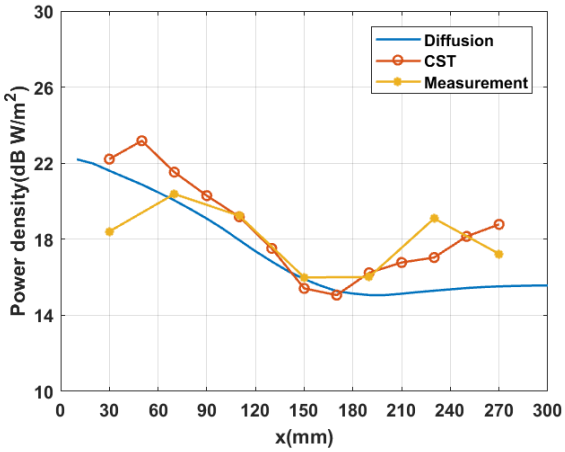

Fig. 14. Power density, normalized to 1W input power, along the central line of the lid of the enclosure loaded with the 90mm cube at 5.5GHz, comparing diffusion model to CST simulation and measurement.

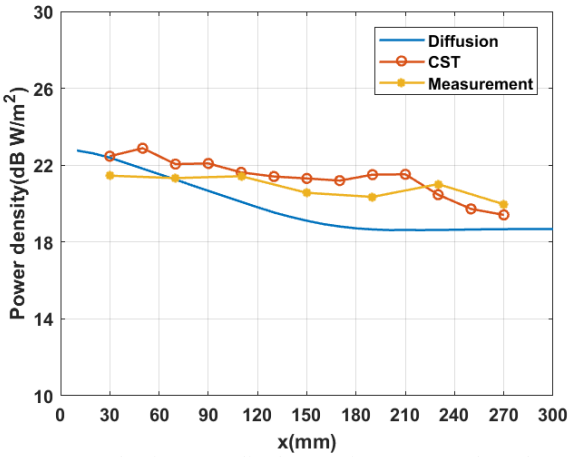

Fig. 15. Power density, normalized to 1W input power, along the central line of the lid of the enclosure loaded with the 70mm cube at 5.5GHz, comparing diffusion model to CST simulation and measurement.

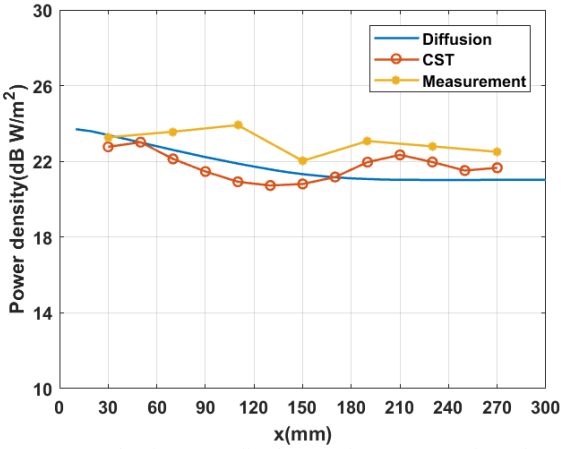

Fig. 16. Power density, normalized to 1W input power, along the central line of the lid of the enclosure loaded with the 55mm cube at 5.5GHz, comparing diffusion model to CST simulation and measurement.

wave simulations and physical measurements with less than 3dB difference. It is obvious that the power density is not uniform along the central line of the enclosure lid due to the

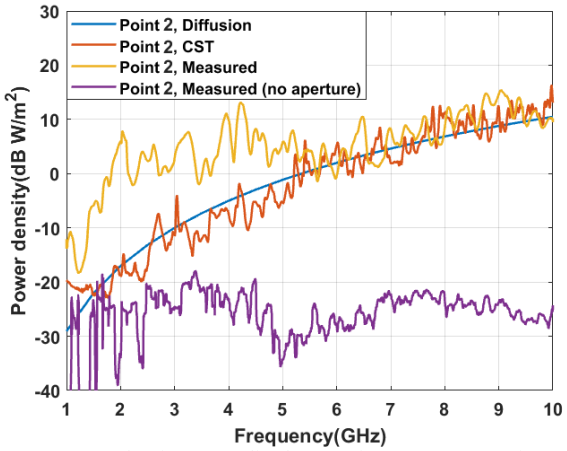

Fig. 17. Power density, normalized to 1W input power, at point 2 (shown in Fig.2) of the enclosure with an r=6mm circular aperture and loaded with the 90mm cube, comparing diffusion model to CST simulation and measurement. Measurement of the same loaded enclosure without aperture is also provided as a reference.

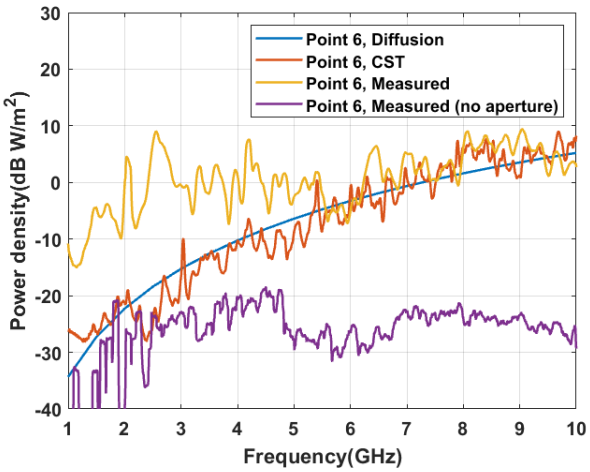

Fig. 18. Power density, normalized to 1W input power, at point 6 (shown in Fig.2) of the enclosure with an r=6mm circular aperture and loaded with the 90mm cube, comparing diffusion model to CST simulation and measurement. Measurement of the same loaded enclosure without aperture is also provided as a reference.

presence of the absorbing cubes and it decays gradually as a function of distance. This decay is rapid at the front part (the space between the aperture and the cube, 0mm<x<120mm). At the rear part (the space behind the cube, 210mm<x<300mm), the power density predicted by the diffusion model does not change much. Since the absorbing cube is at the center of the enclosure, the power density reaches the lowest point at around x=150mm. This is particularly obvious in Fig. 14. As the cube becomes smaller, the drop becomes less obvious as ban be seen in Figs. 15 and 16.

As mentioned in Section III, the cut-off frequency of the 75 mm × 75 mm aperture is 1GHz, which means it has a constant transmission cross section, which is a quarter of its area, throughout the measurement range. Therefore, we also measured the same enclosure, with an r=6mm circular aperture with a cut-off frequency of 10.2GHz, to see what happens when the transmission cross section of the aperture varies with frequency. Figs.17 and 18 show the power density of the enclosure with the circular aperture as a function of frequency. The diffusion model, CST model and measurement set up of this scenario are the same as those shown in Figs. 5, 7 and 10 and they will not be repeated here. The transmission cross section of the circular aperture is calculated by using its polarizabilities (see Table I in [27]). For simplicity, we only show the power densities at point 2 and 6 (shown in Fig. 2). It can be seen that the power density increases with frequency. This is because the transmission cross section of the aperture is frequency dependent between 1GHz -10GHz and it increases with frequency.

Below 5GHz, the measurement is not in agreement with diffusion model and CST. To investigate the cause of this discrepancy, we covered the aperture and measured the power density again. The results are presented in Figs. 17 and 18 with the legend “no aperture”. It can be seen that the power density without the aperture is much lower than that with the aperture. Therefore, we know that the measurements with the aperture are well above the noise floor of the measurement equipment and we can rule out leakage through the joint of the lid. In addition, we investigated the field statistics in the enclosure below 5GHz and found out that the internal field complies with normal distribution (the results are not presented in this paper), which indicates that the field is sufficiently diffuse. Currently we are still not certain about the cause of discrepancy between the measurement and full-wave simulation below 5GHz.

VIII. Conclusion

The diffusion equation based model is a generalization of the traditional PWB method and it is able to account for the field inhomogeneity in highly dissipative spaces. The diffusion model takes longer to reach a solution than the PWB method, but is still time-saving compared to full wave solvers, which enables it to be applied to early stage of EMC design to obtain fast estimations. Initial evaluation has proved the potential of the 2D diffusion model. In this paper, we demonstrated the applicability of the 3D diffusion model by predicting the electromagnetic field in a perforated enclosure loaded with a series of absorbing cubes and comparing with full wave simulations and measurements. The agreement between them is generally good with only a few decibels difference. The 3D model enables more complex applications to be investigated. For instance, it is able to predict the non-uniform field in a populated equipment enclosure, informing the optimal positioning of sensitive components to reduce the influence of electromagnetic interference on them.

An extension of this study would be applying the diffusion model to enclosures with high dimensional ratio (one side is much longer than the other two). In [18], Visentin et al pointed out that for such enclosures the diffusivity along the longest side is no longer a constant. Although some empirical solutions have been proposed, more research is required to verify them.

REFERENCES

[1] A. Taflove and S. C. Hagness, *Computational Electrodynamics: the Finite Difference Time Domain Method*, *3rd edition*. Norwood, MA: Artech House, 2005.

[2] R. F. Harrington, *Field Computation by Moment Methods*. New York, NY: Wiley-IEEE Press, 1993.

[3] C. Christopoulos, *The Transmission Line Modelling Method: TLM.* New York, NY: Wiley-IEEE Press, 1995.

[4] J. Jin, *The Finite Element Method in Electromagnetics, 2nd edition*. New York, NY: Wiley-IEEE Press, 2002.

[5] F. Moglie and A. P. Pastore, "FDTD analysis of plane waves superposition to simulate susceptibility tests in reverberation chambers," *IEEE Trans. Electromag. Compat*., vol. 48, no. 1, pp. 195-202, Feb. 2006.

[6] D. A. Hill, M. T. Ma, A. R. Ondrejka, B. F. Riddle, M. L. Crawford, and R. T. Johnk, "Aperture excitation of electrically large, lossy cavities," *IEEE Trans. Electromag. Compat*., vol. 36, no. 3, pp. 169-178, Aug. 1994.

[7] I. Junqua, J. P. Paramantier, and F. Issac, "A network formulation of the power balance method for high-frequency coupling," *Electromagnetics*, vol. 25, nos. 7-8, pp. 603-622, Feb. 2005.

[8] I. D. Flintoft, S. L. Parker, S. J. Bale, A. C. Marvin, J. F. Dawson, and M. P. Robinson, "Measured average absorption cross section of printed circuit boards from 2 to 20GHz," *IEEE Trans. Electromagn. Compat*., vol. 58, no. 2, pp. 553-560, Apr. 2016.

[9] C. Foy, J. Picaut, and V. Valeau, "Including scattering within the room acoustics diffusion model: an analytical approach," *J. Acoust. Soc. Amer.*, vol. 140, no.4, pp. 2659-2669, Oct. 2016.

[10] L. Savioja, and U. P. Svensson, "Overview of geometrical room acoustic modelling techniques," *J. Acoust. Soc. Amer.*, vol. 138, no.2, pp. 708-730, Aug. 2015.

[11] I. D Flintoft, A. C. Marvin, F. I. Funn, L. Dawson, X. Zhang, M. P. Robinson and J. F. Dawson, "Evaluation of the diffusion equation for modeling reverberant electromagnetic fields," *IEEE Trans. Electromagn. Compat.*, vol. 59, no. 3, pp. 760-769, June 2017.

[12] J. Yan, J. Dawson, and A. Marvin, "Estimating reverberant electromagnetic fields in populated enclosures by using the diffusion model," *2018 IEEE Int. Symp. Electromagn. Compat.*, Long Beach, CA: pp. 363–367.

[13] V. Valeau, J. Picaut, and M. Hodgson, "On the use of a diffusion equation for room acoustic prediction," *J. Acoust. Soc. Amer.*, vol. 119, no.3, pp. 1504-1513, Mar. 2006.

[14] J. Picaut, L. Simon, and J. D. Polack, "A mathematical model of diffuse sound field based on a diffusion equation," *Acta Acustica*, vol. 83, no. 4, pp. 614-621, Jul. 1997.

[15] V. Valeau, M. Hodgson, and J. Picaut, "A diffusion based analogy for the prediction of sound fields in fitted rooms," *Acta Acustica* , vol. 93, no. 1, pp. 94-105, Jan. 2007.

[16] W. C. Sabine, *Collected papers on acoustics*, Harvard University Press, Cambridge, USA, 1922.

[17] J. M. Navarro, and J. Escolano, "Simulation of building indoor acoustics using an acoustic diffusion equation model," *J. Building Perform. Simul*., vol. 8, no. 1, pp. 3-14, Nov. 2013.

[18] V. Visentin, N. Prodi, and V. Valeau, "A numerical investigation of the Fick's law of diffusion in room acoustics," *J. Acoust. Soc. Amer.*, vol. 132, no.5, pp. 3180-3189, Nov. 2012.

[19] A. Billon, C. Foy, J. picaut, and V. Valeau, "Modeling the sound transmission between rooms coupled through partition walls by using a diffusion model," *J. Acoust. Soc. Amer.*, vol. 123, no.6, pp. 4261-4271, Jun. 2008.

[20] X. Zhang, M. P. Robinson, I. D. Flintoft, and J. F. Dawson, "Efficient determination of reverberant chamber time constant," *IEEE Trans. Electromagn. Compat*., vol. 60, no. 5, pp. 1296-1303, Oct. 2018.

[21] I. D. Flintoft, S. J. Bale, A. C. Marvin, M. Ye, J. F. Dawson, C. Wan, M. Zhang, S. L. Parker, and M. P. Robinson, "Representative contents design for shielding enclosure qualification form 2 to 20GHz," *IEEE Trans. Electromagn. Compat.*, vol. 60, no. 1, pp. 173-181, Feb. 2018.

[22] F. Hecht, "New developments in FreeFEM++," *J. Numer. Math*., vol. 20, nos. 3-4, pp. 251-266, Dec. 2012.

[23] Computer Simulation Technology (CST). [Online]. Available: http://www.cst.com.

[24] York Advanced Research Computing Cluster (YARCC). [Online]. Available: http://wiki.york.ac.uk/display/RHPC/YARCC+-+York+Advanced+Research+Computing+Cluster.

[25] *Standard method of measuring the shielding effectiveness of enclosures and boxes having all dimensions between 0.1m and 2m*. IEEE Standard 299.1, 2013.

[26] A. C. Marvin, G. Esposito, J. F. Dawson, I. D. Flintoft, L. Dawson, J. A. K. Everard and G. C. R. Melia, "A wide-band hybrid antenna for use in reverberation chambers," *2013 IEEE Int. Symp. Electromagn. Compat*., pp.222-226, Aug. 2013.

[27] H. A. Mendez, "Shielding theory of enclosures with apertures," *IEEE Trans. Electromagn. Compat.*, vol. 20, no. 2, pp. 296-305, May 1978.